MOLEKUL
eISSN: 2503-0310

Articles
https://doi.org/10.20884/1.jm.2026.21.2.20175

Analytical and Spectral Characterization of Thion-Imine Terminal Ligand with its Chelation Compounds: Fabrication, Diagnosis, and Vital Assessment of Several Microorganisms

Safaudeen Ali Hussain, Enaam Ismail Yousif***

Department of Chemistry, College of Education for Pure Sciences - Ibn-Al-Haitham, University of Baghdad, Baghdad, Iraq

*Corresponding author email: anaam.i.y@ihcoedu.uobaghdad.edu.iq; safaa.ali2205@ihcoedu.uobaghdad.edu.iq

Received April 14, 2026; **Accepted** June 27, 2026; **Available online** July 20, 2026

ABSTRACT. This work reports the formation of a new type of Azo-Schiff fabricated ligand derived from a thiosemicarbazide compound, together with its metal complexes. The ligand, N-(3-((E)-(4-((Z)-1-(2-carbamothioylhydrazineylidene) ethyl)phenyl) diazenyl)-4-hydroxyphenyl) acetamide (HL), was synthesized through condensation of (E)-N-(3-((4-acetylphenyl)diazenyl)-4-hydroxyphenyl)acetamide with thiosemicarbazide by using equivalent molar amounts. This compound was then used as a ligand to coordinate to metal ions, forming complexes with a 1:2 metal-to-ligand ratio. The ligand bonded to the metals via thion and imine groups, with two chlorine bonds on either side, forming octahedral complexes. These compounds were characterized using various spectroscopic, physical, and thermal methods, from which the structural and chemical properties of the resulting compounds were determined. Antimicrobial evaluation against two $G^{(+)}$ bacteria (*Staphylococcus aureus, Streptococcus faecalis*), two $G^{(-)}$ bacteria (*Acinetobacter baumannii, Escherichia coli*), and two species of fungi (*Candida albicans, Candida tropicalis*).

Keywords: Azo-thiosemicarbazone ligand, characterisation, Metal complexes, microbial evaluations.

INTRODUCTION

Azo-Schiff organic substances are among the most striking coordination systems for investigators due to their structural elasticity and ability to form stable Metallic derivatives with transition metal ions (Waszkowska et al., 2025). Groups of the Azo linkage (-N=N-) and the Schiff group (-C=N-) give in the same structure distinctive electronic and structural properties, allowing them to react with metals at multiple sites, such as phenolic oxygen, azomethine nitrogen, or sulphur in thiosemicarbazone. This versatility often leads to the formation of highly thermally and chemically stable coordination compounds (Ali & Hassan, 2025). These complexes have unique electronic transitions in UV-Vis spectra, indicating the coordinated nature of their bonds (Elbadawy et al., 2025). Recent studies indicate that Schiff base compounds of chromium(III), iron(III), nickel(II), and copper(II), in addition to their use as pharmaceutical or biomaterials, also exhibit semiconductor properties suitable for electronic applications (Mousa et al., 2025). Moreover, several complexes have exhibited antioxidant properties, hence increasing their significance in chemical and medicinal applications (Sarwade et al., 2025). Azo-Schiff chemicals and their complexes are utilized in dyes and polymers owing to their chromatic properties and thermal stability (Siotey et al., 2025).Their catalytic capabilities render them formidable candidates for industrial catalytic processes, including the oxidation of organic molecules and polymerization reactions (Lakhani et al., 2024).Recent research has suggested their possible application in the development of novel materials for solar cells and electronic gadgets (Mughal et al., 2026). This project seeks to synthesize a novel Azo-Schiff ligand derived from azo moiety and thiosemicarbazone, and examine its capability to form stable complexes with the transition metal ions Cr(III), Fe(III), Ni(II), and Cu(II). Characterize the synthesized compounds utilizing spectroscopic techniques (UV-Vis, FTIR, NMR), along with magnetic, thermal, and physical studies to validate the postulated octahedral configuration. The biological activity of the linker and its compounds was evaluated against specific types of $G^{(+)}$ and $G^{(-)}$ bacteria, as well as two species of fungi, to study their possible use as antimicrobial agents.

EXPERIMENTAL SECTION

Materials and Procedures

NMR analysis (^{1}H, ^{13}C) of HL was obtained by Bruker-300_{MHz} spectrometer, in $DMSO_{d_6}$ as a solvent and Tetramethylsilane as a control reference for the 1H NMR analysis. FTIR spectra were detected by

4000–200 cm^{-1} region using KBr/CsI2. Positive charge electrospray ionization mass spectra were obtained with a Sciex ESI instrument. Melting points were determined on a Stuart SMP40 electrothermal apparatus. UV–Vis's absorption measurements were carried out using a Shimadzu UV-Visible 160A spectrophotometer, scanning from 200 to 1000 nm. Solutions of the samples were obtained in DMSO at a concentration of 1.0 x 10^{-3} - 1.0 x 10^{-5} mol L^{-1} and placed in a quartz cuvette (1 cm path length) at ambient temperature. Conductivity was performed at 25 °C with a CyberScan CON 510 digital conductivity meter (Eutech Instruments), with DMSO solutions of concentration1.0 x 10^{-3} M. Elemental analysis (C, H, N), metal content, and chloride determination were conducted with a Heraeus Vario EL analyser, a Shimadzu AA 7000 atomic absorption spectrometer, and a potentiometric titration system (Metrohm 686 Titro Processor with a 665 Dosim unit), respectively. Thermal gravimetric studies were examined employing an STA PT-1000 Linseis Thermal Analyser. Magnetic susceptibility was measured at 33 °C using a Johnson Matthey magnetic balance.

Synthesis

A two-step procedure was implemented to obtain the azo Schiff base as follows;

Synthesis of (E)-N-(3-((4-acetylphenyl)diazenyl)4-hydroxyphenyl) acetamid

The experimental procedure was adapted from established methods described in the literature (Mezher & Yousif, 2025b). The preparation of azo dye was as follows: A 250 mL round-bottomed flask was filled it with 4-aminoacetophenone (1.35 g, 10 mmol) and sodium nitrite (0.69 g, 10 mmol). Then, 20 mL of a 1:1 (v/v) ethanol-water mixture was added. Following this, 36% hydrochloric acid solution (2 mL in 10 mL of water) was gradually added to the mixture over the progression of one hour after cooling it in an ice bath at a temperature between 0 and 5 °C. A solution of 4-hydroxyacetanilide (1.51 g, 10 mmol) in 20 mL of ethanol, enhanced with a solution of sodium hydroxide (0.8 g, 20 mmol) in 20 mL of ethanol, was added to the resulting diazonium salt. The reaction mixture was stirred for two hours. The final product was precipitated by adding 100 mL of water and 5 mL of 36% hydrochloric acid solution until a purple precipitate formed. and the solid product was collected by filtration at pH 4 and washed several times with water. The final product was washed with 5 mL of cold ethanol and then air-dried. The yield was 2.04 g (69%), and the melting point of the ligand was 230 °C.

Synthesis of the Ligand N-(3-((E)-(4-((Z)-1-(2-carbamothioylhydrazineylidene)ethyl) phenyl) diazenyl)- 4-hydroxyphenyl)acetamide (HL)

According to the reported synthetic procedure (Mezher & Yousif, 2025a) (Dilawer Issa & Rasul Braiem, 2022), the preparation of HL was carried out. Firstly, a mixture made of thiosemicarbazide (0.091 g, 1.0 mmol) and 10 mL of ethanol, enriched with the addition of three drops of glacial acetic acid, was poured gradually, to (E)-N-(3-((4-acetylphenyl) diazenyl)-4-hydroxyphenyl) acetamide (0.297g, 1.0 mmol), previously dissolved in 20 mL of an ethanol/DMF (3:1, v/v) mixture. The mixture was heated with reflux at 65 °C for 4 h. The hot solution was filtered, and the curd was left to slowly evaporate the solvent at room temperature. Upon cooling, a purple precipitate formed, which was isolated and subsequently recrystallized from ethanol. The purified compound was dried at room temperature. HL was isolated in 0.139g yield (63%), melting point 245 °C.

Synthesis of complexes

A process similar to that used in the preparation of chromium(III) has been used to prepare other metallic compounds, as follows: To a 100 mL round flask containing HL (0.540 g, 2 mmol) dissolved in 10 mL of a mixture of ethanol and DMF at a volumetric ratio of approximately 1:3, 10 mL ethanolic potassium hydroxide (0.16g,3mmol) was added. Subsequently, $CrCl_3 \cdot 6H_2O$ (0.266 g, 1 mmol) in 5 mL of ethanol was added with stirring dropwise. After refluxing the mixture for 2h, the resulting solid was filtrated, washed with 5 mL ethanol, and left to dry. The Cr(III) complex was isolated in a 0.558 g yield (61%) and exhibited a melting point above 300 °C (decomposition). Further details, including isolated masses, observed coloration, metal chloride quantities, and melting points of the coordination compounds, were illustrated in **Table 1**.

Microbiological Evaluation

The disk diffusion technique, as designated by Kirby and Power, was used to assess the antimicrobial efficiency of the synthesized compounds. Microbial suspensions were fixed to match the 0.5 McFarland standard by dilution with 85% sodium chloride solution. The prepared inoculate were evenly spread across the surface of Mueller–Hinton agar plates. Wells of uniform size and spacing were then created in the agar, into which 1 × 10^{-6} L of each sample (1 mg/mL in DMSO) was presented. Plates were incubated at 37 °C for 24 h, after which the inhibition zones were measured and compared with those of the standard drugs (Kasim Mohammed, 2023) (Kasim Mohammed, 2023). Control assays with DMSO alone demonstrated that the solvent possessed no detectable antimicrobial effect on any of the bacterial or fungal species examined. Biological efficacy was evaluated against six microorganisms: two $G^{(+)}$ bacteria (*Staphylococcus aureus, Streptococcus faecalis*), two $G^{(-)}$ bacteria (*Acinetobacter baumannii, Escherichia coli*), and two fungi (*Candida albicans, Candida tropicalis*). The results were compared with those of a common drug, penicillin.

Table 1. General physical properties of the coordination compounds.

compound	Amount of metal salt (g)	Isolated complex (g)	Colour	m.p. (°C)	Yield (%)
$[Cr(HL)_2Cl_2]ClH_2O$	0. 266	0.558	Dark brown	>300*	61
$[Fe(HL)_2Cl_2]ClH_2O$	0. 162	0.541	brown	>300*	59
$[Ni(HL)_2Cl_2]\ H_2O$	0.237	0.506	Greenish yellow	>300*	57
$[Cu(HL)_2Cl_2].H_2O$	0.170	0.517	Dark brown	>300*	58

RESULTS AND DISCUSSION

The reaction of (E)-N-(3-((4-acetylphenyl)diazenyl)-4-hydroxyphenyl) acetamide with thiosemicarbazide in a 1:1 molar ratio in ethanol (**Scheme 1**) resulted in the preparation of the new azo Schiff base, N-(3-((E)-(4-((Z)-1-(2-carbamothioylhydrazineylidene)ethyl)phenyl) diazenyl) -4-hydroxyphenyl) acetamide (HL). In this aromatic system, the phenolic hydroxyl group site is unavailable for electrophilic substitution; therefore, azo coupling occurs at the ortho-like C-3 position. This ligand has many terminals that can play as chelate position. In this work, sulphur of thion and nitrogen of Schiff imine group were bonded with metal ions. Ligand was subsequently treated with Cr(III), Fe(III), Ni(II), and Cu(II), each provided as the corresponding chloride salt, in a 2:1 ligand-to-metal molar ratio to yield the respective coordination complexes. The isolated paramagnetic complexes of the general formulae $[M(HL)_2Cl_2]Cl{\cdot}H_2O$ (M(III)=Cr and Fe), $[M(HL)_2Cl_2]\ H_2O$ (M(II)= Ni, and Cu) are depicted in **Scheme 2**. The experimental microanalysis results, including metal and chloride contents, agree well with the calculated values in **Table 2**. $[Cr(HL)_2Cl_2]Cl{\cdot}H_2O$ and $[Fe(HL)_2Cl_2]Cl{\cdot}H_2O$ complexes are electrolytes, according to molar conductance measurements in DMSO solutions, apart from the $[Ni(HL)_2Cl_2]{\cdot}H_2O$ and $[Cu(HL)_2Cl_2]{\cdot}H_2O$ complexes, which showed nonelectrolyte properties.

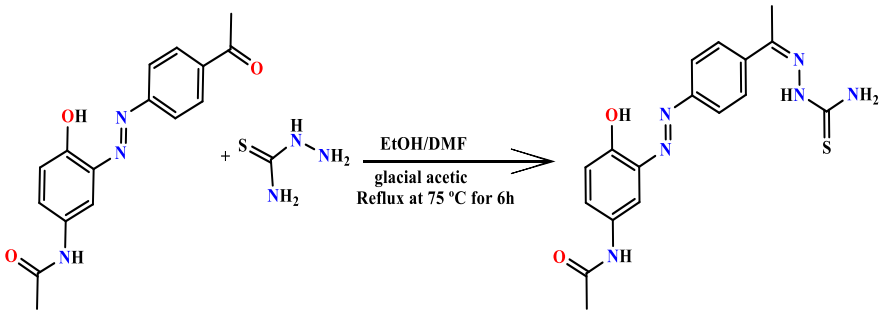

Scheme 1. General synthetic route of HL

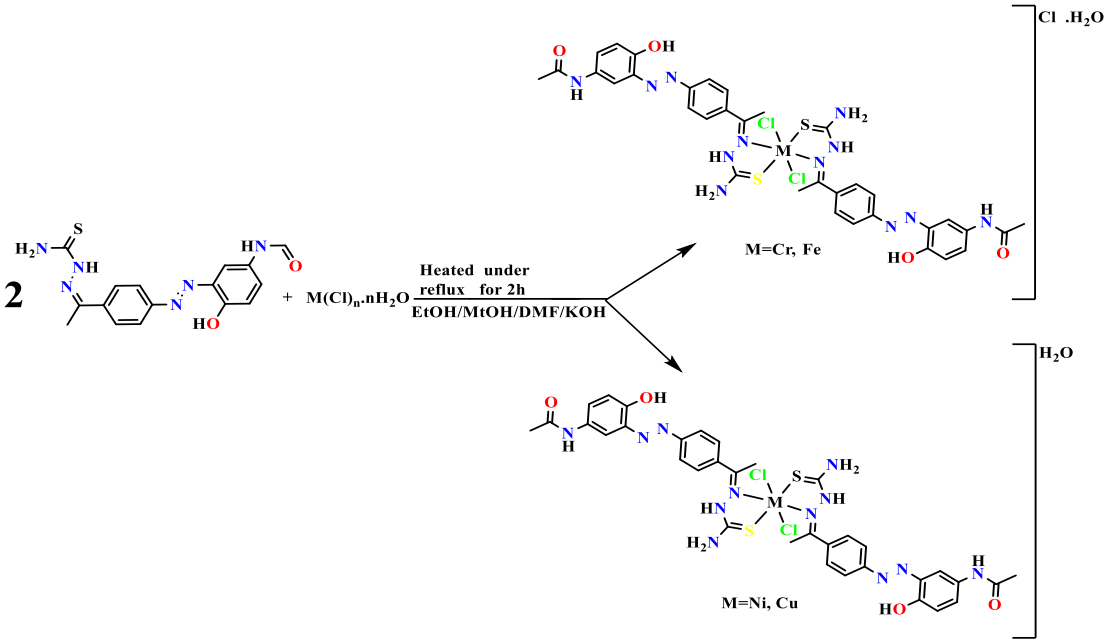

Scheme 2. Proposed structures of metal complexes

Table 2. Elemental microanalysis, metal and chloride content of complexes.

compound	$M_{g/mol}$	Element analysis cal./fou.				
		C (%)	H (%)	N (%)	Cl (%)	Metal %
HL	370.43	55.12 55.30	4.90 4.99	22.69 22.41	-	-
$[Cr(HL)_2Cl_2]ClH_2O$	916.21	44.57 44.62	4.07 4.02	18.35 18.40	11.61 11.58	5.68 5.71
$[Fe(HL)_2Cl_2]ClH_2O$	918.08	44.39 44.44	4.05 4.07	18.27 18.31	11.56 11.60	6.07 6.04
$[Ni(HL)_2Cl_2]\ H_2O$	888.47	45.96 45.68	4.31 4.33	18.82 18.79	7.98 7.92	6.61 6.77
$[Cu(HL)_2Cl_2].H_2O$	893.32	45.71 45.75	4.29 4.26	18.82 18.85	7.94 7.97	7.11 7.14

NMR Spectra

The ^{1}H NMR spectrum (300 MHz, $DMSO_{d6}$) of the HL (**Figure 1**) shows three downfield singlets at δ 10.73, 10.32, and 9.93 ppm. Each signal integrates for one proton. These resonances are characteristic of strongly deshielded, exchangeable protons and are assigned to the phenolic OH and the two amide N-H protons (N-H_{-15} and N–H_{-23}), respectively. The marked downfield shifts reflect the influence of intra-or intermolecular hydrogen bonding, either with $DMSO_{d6}$ or within the molecular framework. A well-defined doublet is observed at δ 8.17–8.14 ppm (2H, J = 8.49 Hz), corresponding to the aromatic protons H_{-C11} and H_{-C12}. A singlet at δ 8.04 ppm is attributed to the NH_2 group. Another aromatic doublet appears at δ 7.98–7.96 ppm (2H, J = 8.40 Hz), assigned to H_{-C14} and H_{-C10}. The proton H_{-C2} gives a doublet at δ 7.59–7.56 ppm (J = 8.52 Hz, 1H), while H_{-C3} resonates as a doublet at δ 7.03–7.00 ppm (J = 8.94 Hz, 1H). Two methyl groups appear as singlet signals at δ 2.36 ppm and 2.03 ppm, each integration to three protons, and are assigned to CH_3-17 and CH_3-21, respectively (**Figure 1**). Residual solvent signals are observed at δ 2.50 ppm ($DMSO_{d6}$) and δ 3.32 ppm (traces of water). ^{13}C NMR (75 MHz, $DMSO_{d6}$) spectrum (**Figure 2**) shows a group of peaks lying in the downfield region that belongs to phenolic, amidic, and thionic carbon atoms located at 181.57, 179.44 and 168.59 ppm, respectively, because of the high deshielding force. Electronic withdrawing effect led nuclei of C_4, C_{20}, C_9, and C_1 resonances to be observed at 152.16, 151.60, 147.29, and 140.46 ppm, respectively. The signals at 138.51 and 132.33 ppm are attributed to the C_3 and C_5 frequencies, while the other two assignments, which appeared at 128.31 and 128.14 ppm, could be related to the C_{10} and C_{14} nuclei because they have the same chemical shifts. The rest of the aromatic region could show peaks at 123.04, 118.69, and 111.96 ppm, which belong to C_6, C_{11}, and C_{13} frequencies. The aliphatic region shows the two peaks of the methylene group C_{17} and C_{21}, at 24.31 and 14.46 ppm. Finally, the solvent peak DMSO appeared around 40 ppm.

Mass Spectra

The electrospray mass spectrum and suggested fragmentation for HL displayed by **Figure 3**, **Scheme 3**, illustrated the parent peak (m/z) at 370.80 g/mol, which related to major product. Formic acid was used as positive charge enhancer, with acetonitrile as solvent. Because of that, Another peak observed at 411.95 g/mol could be related to (M^+ trace of solvent) (Holness & Almirall, 2013; Muggli & Schürch, 2024). The rest of moieties cracks were noticed at 290.95; 232.90; 214.95; 145.90; 100.00 g/mol which could be related to theoretically Molecular mass :290.36; 232.27; 145.18; 100.14 g/mol with proposed Chemical Formulas: $C_{13}H_{16}N_5OS^+$, $C_{11}H_{14}N_5O+$, $C_{12}H_{12}N_3O^+$, $C_9H_9N_2^+$, $C_5H_{10}NO^+$.

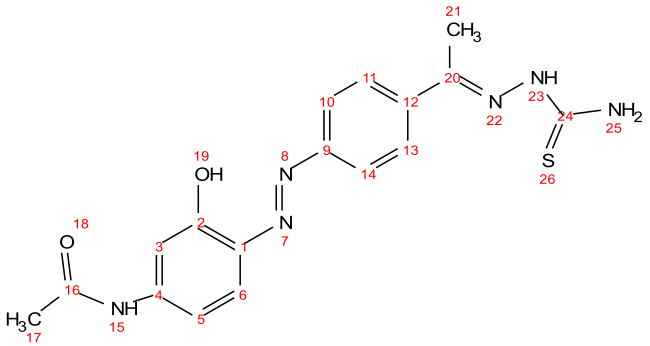

Scheme 3. Labelling of ligand atoms

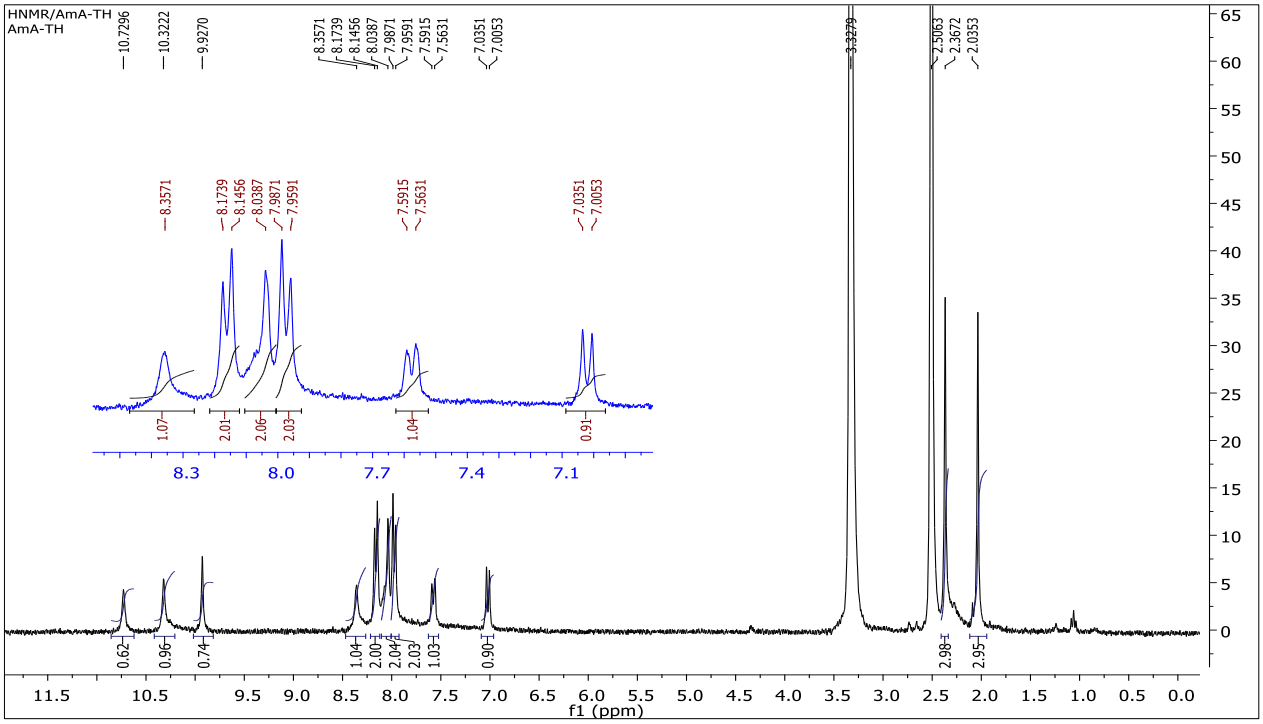

Figure 1. ^{1}HNMR spectrum HL

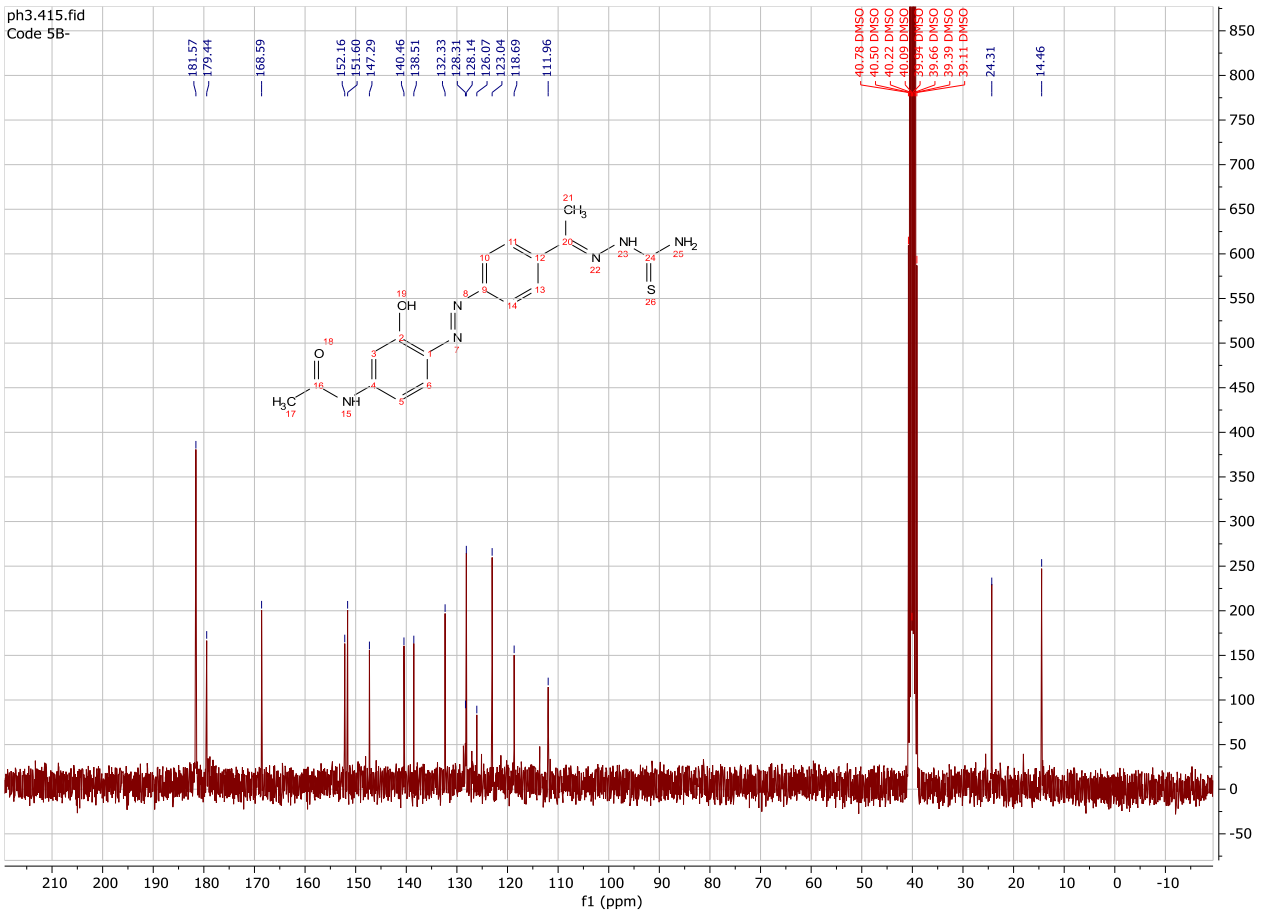

Figure 2. ^{13}CNMR spectrum HL.

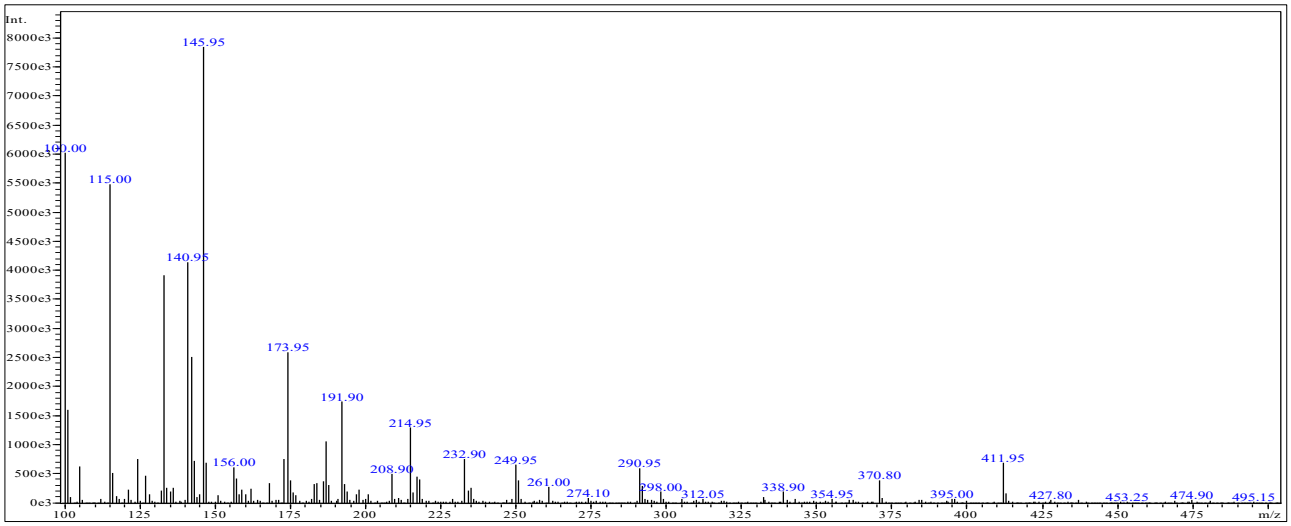

Figure 3. ESI. Mass spectrum for HL

Table 3. Infrared spectroscopic information HL also its metal chelates (cm^{-1}).

Derivates	$(O-H)_{St}$ H_2O	$(N-H_2)_{St}$	$(N-H)_{amd}$	ν(C=O)	$ν(C=N)_{imi}$	$(C=C)_{aro.}$	ν(N=N)	(C=S)	(M-N)	(M-S)	(M-Cl)
HL	3473	3373	3263 3174	1668	1618	1560	1487	1163 995	-	-	-
$[Cr(HL)_2Cl_2]Cl.H_2O$	3444 3419	3369	3240 3169	1668	1606	1550	1490	1141 964	414	334	273
$[Fe(HL)_2Cl_2]Cl\ H_2O$	3581 3448	3319	3246 3151	1668	1604	1564	1490	1141 964	416	337	250
$[Ni(HL)_2Cl_2]\ H_2O$	3487 3437	3292	3161 3107	1662	1600	1558	1490	1145 985	426	318	260
$[Cu(HL)_2Cl_2]\ H_2O$	3460 3410	3336	3236 3150	1674	1589	1566	1487	1131 956	418	329	266

FTIR Spectra

The main infrared peaks of the derivatives are displayed along with their values in **Table 3.** In the HL spectrum, a frequency detected at 3473 cm^{-1} appears to be related to the stretching of the phenol group ν(OH) (Ismail Yousif et al., 2026). The bands recorded at 1668 and 1487 cm^{-1} correspond to the ν(C=O) stretching modes of carbonyl and the ν(N=N) of azo linkage, respectively (Hamza & Yousif, 2023). The appearance of a new peak at 1618 cm^{-1} indicates the formation of a new moiety, double imine bond (C=N). The complexes exhibited a distinct FTIR spectral shift. The imine peak shifting to frequencies revealed at 1606, 1604, 1600, and 1589 cm^{-1}, while the thionyl peaks shifted to 1141,964, 1141,965, 1145,985, and 1131,956 cm^{-1} to the Cr(III), Fe(III), Ni(II), and Cu(II) complexes, respectively. Metal's association with thion's sulfide and nitrogen of imine is illustrated by peaks at 334, 414, 337, 416, 318, 426, and 329, 418cm^{-1} in the complexes of Cr(III), Fe(III), Ni(II), and Cu(II), respectively(Al-Gaber et al., 2023). FTIR (near-IR) spectra using CsI_2 disks clearly showed peaks for the metal's association with a chlorine atom, observed at 273, 250, 260, and 266 cm^{-1}, respectively (Al-Gaber et al., 2023; Atallah & Ahmed, 2025).

Electronic Spectra

The magnetic moment values and UV-visible spectral data for the ligand and complexes are summarized in **Table 4**. Peaks detected between 224-299nm and in the range 319-439nm in the spectra of the complexes are correlated to the ligand field ($\pi\rightarrow\pi^*$ and $n\rightarrow\pi^*$) and charge transfer transitions, respectively (Cozzi, 2004)(Subha et al., 2016). The spectrum of the $Cr^{(III)}$ complex shows a distinctive peak at 599nm corresponding to the $^4A_2g\rightarrow\ ^4T_1g^{(F)}$, suggesting a distorted octahedral arrangement around the Cr(III) center. This explanation is supported further by the μ_{eff} value of 3.81 BM for the Cr(III) complex (Al-Jeboori et al., 2008). This value is close to the expected spin-only moment for a high-spin d^3 ion (3.87 BM), supporting the assigned geometry. The Fe(III) complex exhibits a peak at 510 nm assigned to the $^3A_2g^{(F)}\rightarrow\ ^3T_2g^{(F)}$transition, pointing to an octahedral geometry at the Fe(III) site, which is in agreement with the measured magnetic moment of 5.65 BM(Al-Jeboori et al., 2008)(Hossain et al., 2022). This is consistent with the spin-only value for a high-spin d^5 Fe(III) center (5.92 BM). The octahedral geometry around the Ni(II) ion is suggested due to that value. This is based on a peak detected at 510 nm, which is

assigned to the $^3A_2g^{(F)} \rightarrow {}^3T_1g^{(p)}$. The observed magnetic moment 2.77BM is consistent with an octahedral configuration around the $Ni^{(II)}$ ion, and that correlated with the ideal moment 2.83 BM (Hameed & Al-Jeboori, 2025)(Lever, 1984). A peak at 597 nm in the spectrum of Cu-complex is linked to the $^4T_1g^{(F)} \rightarrow {}^4A_2g^{(F)}$ transition, revealing a Jahn–Teller distorted octahedral geometry at the Cu site (Nandaniya et al., 2024)(Lever, 1984)(Al-Jeboori et al., 2008). A practical amount magnetic was 1.86 BM for the Cu(II) complex, and that agreed with the theoretical value (1.73 BM), which suggested a structural interpretation (Lever, 1984).

Thermal Analysis

The heat degradation of the ligand, illustrated by **Figure 4**, displayed several infringement phases; the initial segment, at 5% (0.15 mg), may match to the elimination of remaining absorbed water (Mezher & Yousif, 2026).The consequent phase involved a termination of 20% (0.6 mg), due to the suggested partition CH_4N_2S. Another possible portion, 30% (1.05 mg), relates to the $C_8H_8N_2$ moiety. The fourth part step nominated for fracture is 15% (0.45 mg); this fragment can be epitomized as C_2H_4NO. The deposit C_6H_5O represented 25% (0.75 mg). On the other hand, the organic section of the copper complex showed thermal cracking, leaving metal oxide (**Figure 5**). The loss of approximately 1.9% (0.044 mg) around 70- 130 ℃ is ascribed to the loss of hydrous water (Cheng et al., 2019). The heating assortment of 130-210 ℃ is responsible for a mass loss of nearly 26% (0.61 mg) of the $C_{10}H_{10}N_4O_3$ portion complex. Seventeen percent (0.41) was eliminated from the complex moiety upon contact to temperatures between 210 and 330 ℃, attributable to $C_6H_9N_4O$. The remaining chemical molecule $C_{18}H_{16}C_{l2}N_4S_2$ may be eliminated by heating upon approximately 800 ℃. The remaining 0.08% of the mass may be attributed to the metal oxide that exists outside the device's heating range.

Table 4. UV-VIS electronic data of the compounds, magnetic properties and molar conductivity in DMSO.

Derivates	λ_{nm}	E_{MAX} ($dm^3mol^{-1}cm^{-1}$)	Transitions	μeff (BM)	Λ_m $S.cm^2.mole^{-1}$	Suggested geometry
HL	331 448	1883 657	$\pi \rightarrow \pi^*$ $n \rightarrow \pi^*$	-	16.5	-
[Cr $(HL)_2Cl_2$]Cl H_2O	265 381 599	810 298 110	$\pi \rightarrow \pi^*$, C.T $^4A_2g \rightarrow {}^4T_1g^{(F)}$	High field 3.81	35.2	Distorted octahedral
[Fe$(HL)_2Cl_2$]Cl H_2O	228 314 510	1250 170 70	$\pi \rightarrow \pi^*$ C.T $^3A_2g^{(F)} \rightarrow {}^3T_2g^{(F)}$	High field 5.65	46.5	Distorted octahedral
[Ni $(HL)_2Cl_2$] H_2O	224 360 510	1410 2450 150	$\pi \rightarrow \pi^*$ C.T $^3A_2g^{(F)} \rightarrow {}^3T_1g^{(p)}$	High field 2.77	17.99	Distorted octahedral
[Cu $(HL)_2Cl_2$] H_2O	299 439 597	1370 490 280	$\pi \rightarrow \pi^*$ C.T $^4T_1g^{(F)} \rightarrow {}^4A_2g^{(F)}$	High field 1.81	18.03	Distorted octahedral

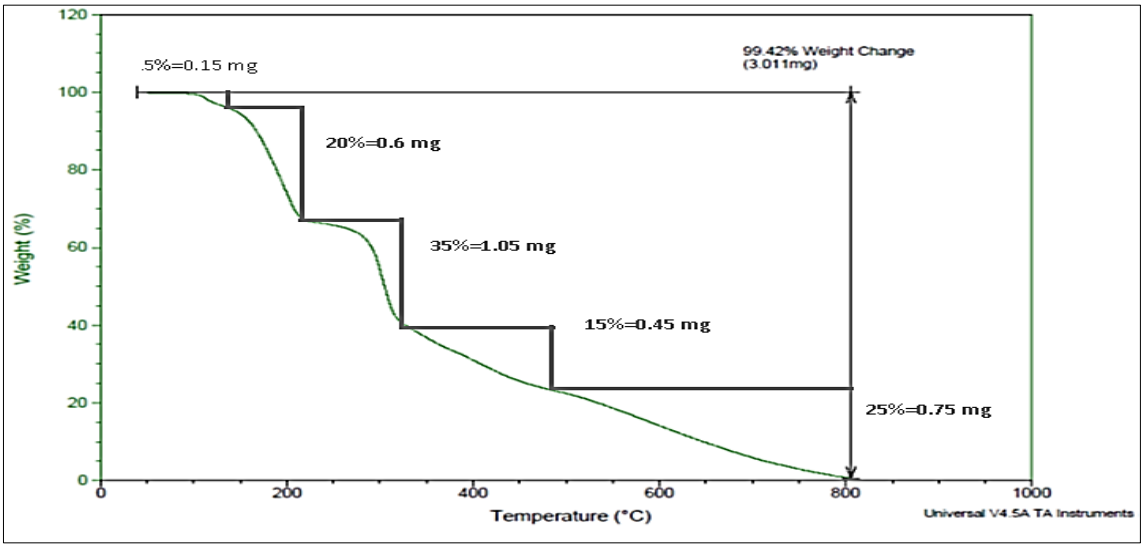

Figure 4. Thermogram of HL.

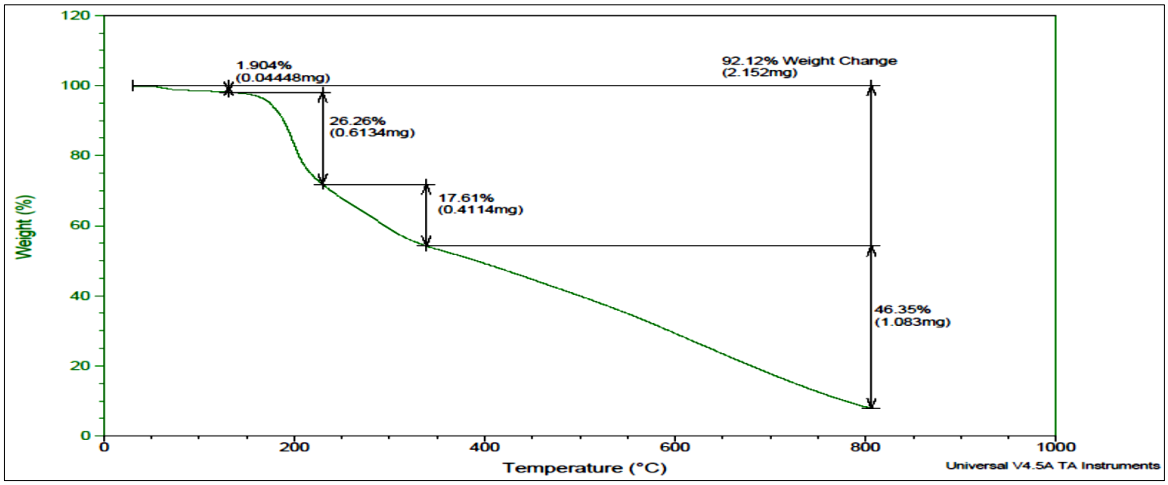

Figure 5. Thermogram of $[Cu(HL)_2Cl_2]\ H_2O$

Table 5. Result of the biological evaluation for synthesis compound.

Sample	Biological activity (inhibition diameter) measured in millimeters					
	$G^{(+)}$ Bact.		$G^{(-)}$ Bact.		Fungi type	
	S.aureus	*S. faecalis*	*A.baumanii*	*E. coli*	*C. albicans*	*C. tropicalis*
HL	0	0	13	0	0	0
$[Cr(HL)_2Cl_2]\ Cl\ H_2O$	13	11	13	0	0	0
$[Fe\ (HL)_2Cl_2]\ Cl\ H_2O$	20	18	0	0	0	0
$[Ni\ (HL)_2Cl_2]\ H_2O$	23	0	12	0	0	0
$[Cu\ (HL)_2Cl_2]\ H_2O$	0	0	0	0	0	0
Penicillin	0	0	0	0	0	0

Microbial Evaluation

In general, the results showed that the complexes were superior to the ligand in effectiveness, and that positive bacteria were more affected than negative bacteria or fungi. The apparent antimicrobial activity of metal derivatives compared to ligands can be explained by the Tweedy theory of chelation (Schatz et al., 1962). According to this theory, chelation reduces the polarity of the ionic metal by partially sharing the positive signal with donors such as nitrogen, oxygen, and sulphur to the ligand, through the delocalization of pi electrons around the chelating ring. This reduction in polarity increases the lipophilic properties of the complex, which then begins to penetrate the lipid layers of the microorganism's cells. Based on Overton theory of cell permeability, the lateral pathway of lipid layer dissolution is a factor influencing antimicrobial activity (Kleinzeller, 1999). The nickel complex exhibited high lipophilicity, which facilitated its penetration of bacterial cell walls. Once inside, the complexes inhibit metabolic pathways by binding to DNA or disabling the switch of respiratory enzymes, which explains the inhibition zones at 23mm (Singha et al., 2023). The difference in activity between $G^{(+)}$ *S. aureus* and $G^{(-)}$ *Escherichia coli* can be explained by differences in cell wall composition. *E. coli* possesses a thick layer of lipopolysaccharides that acts as a barrier against large hydrophobic molecules (Raina & Klein, 2025). Conversely, the absence of this membrane in *E. coli* in *S. aureus* allows the chelating properties of the Azo-Schiff complex to facilitate efficient cell-cell interaction (Franco et al., 2022)(Shu & Mi, 2022). Overall, the results were better compared to penicillin **Table 5**.

CONCLUSIONS

Compound N-(3-((E)-(4-((Z)-1-(2-carbamothioyl hydrazineylidene) ethyl) phenyl) diazenyl)-4-hydroxyphenyl)acetamide was prepared. It was then used as a chelating agent to prepare a range of metallic compounds, and all the prepared compounds were characterized using physical and spectroscopic techniques. The outcomes showed that the metallic compounds formed octahedral shapes around the central metal. Six types of microorganisms were then used: Two types of each: $G^{(+)}$ / $G^{(-)}$ bacteria, in addition two fungi type. This work showed that the complexes were superior to the ligands in their relative activity, while they had no effect on the $G^{(-)}$ bacteria and fungi.

ACKNOWLEDGEMENTS

The authors would like to express their sincere gratitude to the Head of the Chemistry Department and the Dean of the College of Education for Pure Sciences/Ibn Al-Haitham for their support in conducting this study.

REFERENCES

Al-Gaber, M. A. I., Abd El-Lateef, H. M., Khalaf, M. M., Shaaban, S., Shawky, M., Mohamed, G. G., Abdou, A., Gouda, M., & Abu-Dief, A. M. (2023). Design, synthesis, spectroscopic inspection, DFT and molecular docking study of metal chelates incorporating azo dye ligand for biological evaluation. *Materials*, *16*(3), 897.

Al-Jeboori, M. J., Abdul-Ghani, A. J., & Al-Karawi, A. J. (2008). Synthesis and structural studies of new Mannich base ligands and their metal complexes. *Transition Metal Chemistry*, *33*(7), 925–930.

Ali, F. R., & Hassan, H. A. (2025). Azo-Schiff type ligands derived from curcumin and their complexes with transition metals, synthesis, characterization and bioactivity studies. *Baghdad Science Journal*, *22*(10), 3252–3268.

Atallah, S. I., & Ahmed, F. J. (2025). Synthesis and characterization of a novel Schiff base and its complexes with cobalt (II), nickel (II), copper (II), and zinc (II): Spectroscopic study and evaluation of biological activity. *Bani Waleed University Journal of Humanities and Applied Sciences*, *10*(3), 1–12.

Cheng, L., Li, W., Li, Y., Yang, Y., Li, Y., Cheng, Y., & Song, D. (2019). Thermal analysis and decomposition kinetics of the dehydration of copper sulfate pentahydrate. *Journal of Thermal Analysis and Calorimetry*, *135*(5), 2697–2703.

Cozzi, P. G. (2004). Metal–Salen Schiff base complexes in catalysis: practical aspects. *Chemical Society Reviews*, *33*(7), 410–421.

Dilawer Issa, K., & Rasul Braiem, R. (2022). Green and highly efficient synthetic approach for the synthesis of 4-aminoantipyrine Schiff bases. *Chemical Review and Letters*, *6*(1), 2–6.

Elbadawy, H. A., Eldissouky, A., El-Apasery, M. A., Elsayed, D. S., & Alaswad, E. A. (2025). Synthesis, characterization, computational and dyeing behavior of Cu (II) and Zn (II) metal complexes derived from azo-Schiff bases containing phenol derivatives. *BMC Chemistry*, *19*(1), 207.

Franco, D., Calabrese, G., Guglielmino, S. P. P., & Conoci, S. (2022). Metal-based nanoparticles: antibacterial mechanisms and biomedical application. *Microorganisms*, *10*(9), 1778.

Hameed, M. A., & Al-Jeboori, M. J. (2025). Synthesis, characterization, and antimicrobial evaluation of a new bis (semicarbazone) ligand and its coordination complexes. *Synthesis*, *13*, 14.

Hamza, M. B., & Yousif, E. I. (2023). New metal complexes derived from azo linked Schiff-base ligand: Synthesis, spectral investigation and biological evaluation. *Journal of University of Anbar for Pure Science*, *17*(2).

Holness, H., & Almirall, J. (2013). Speciation effects of solvent chemistry on the analysis of drugs and explosives by electrospray ion mobility mass spectrometry. *International Journal for Ion Mobility Spectrometry*, *16*(3), 237–246.

Hossain, M. S., Khushy, K. A., Latif, M. A., Hossen, M. F., Asraf, M. A., Kudrat-E-Zahan, M., & Abdou, A. (2022). Co (II), Ni (II), and Cu (II) complexes containing isatin-based Schiff base ligand: synthesis, physicochemical characterization, DFT calculations, antibacterial Activity, and molecular docking analysis. *Russian Journal of General Chemistry*, *92*(12), 2723–2733.

Ismail Yousif, E., Ibrahim Ahmed, A., & Al-Jeboori, M. J. (2026). Synthesis, characterisation, thermal analysis and antimicrobial evaluation of an azo–Schiff base derived from 4-aminoantipyrine and its selected transition metal complexes. *Bulletin of Pharmaceutical Sciences Assiut University*, *49*(1), 237–255.

Mohammed, B. K., & Yousif, E. I. (2023). Synthesis, structural characterisation and biological activity; new metal complexes derived from semicarbazone ligand. *Revista Bionatura*, *8*(2), 14.

Kleinzeller, A. (1999). Charles Ernest Overton's concept of a cell membrane. *Current topics in membranes*, 48, 1–22)

Lakhani, P., Bhanderi, D., & Modi, C. K. (2024). Nanocatalysis: recent progress, mechanistic insights, and diverse applications. *Journal of Nanoparticle Research*, *26*(7), 148.

Lever, A. B. P. (1984). Electronic spectra of dn ions. *Inorganic Electronic Spectroscopy*, *2*, 376–611.

Mezher, M. Q., & Yousif, E. I. (2025a). New metal complexes with azo-Schiff base ligand synthesis, characterisation and biological activity. *Proceedings of the 13th International Conference on Appliedon Applied Innovations in IT (ICAIIT)*, *13*(2), 643–652.

Mezher, M. Q., & Yousif, E. I. (2025b). Synthesis, spectral characterisation and biological evaluation of a new azo-ligand derived from aminoacetophenone with its metal complexes. *Proceedings of the International Conference on Applied Innovations in IT (ICAIIT)*, *13*(2), 623–633.

Mezher, M. Q., & Yousif, E. I. (2026). CrIII, MnII and CoII complexes with Schiff base ligand; Synthesis, characterization, physicochemical and thermal properties. *Ibn AL-Haitham Journal For Pure and Applied Sciences*, *39*(1), 227–237.

Mousa, E., Tammam, A. K., Refaat, A. M., & Mohamed, G. G. (2025). Integrated analysis of nano Schiff base complex for bioelectronic applications. *Scientific Reports*, *15*(1), 31202.

Muggli, T. M., & Schürch, S. (2024). Influence of solvent relative permittivity in swab spray mass spectrometry. *Molecules*, *29*(17), 4274.

Mughal, E. U., Naeem, N., Al-Rooqi, M. M., Kainat, S. F., Samman, S. S., Alsimaree, A. A., Sadiq, A., Ashiq, S., & Ahmed, S. A. (2026). Recent advances in azo-based metal complexes: structural design, photonic performance, and electrochemical applications. *Journal of Inorganic and Organometallic Polymers and Materials*, 1–41.

Nandaniya, B. K., Das, S. P., Chhuchhar, D. R., Pithiya, M. G., Khatariya, M. D., Jani, D., & Dangar, K. B. (2024). Schiff base metal complexes: Advances in synthesis, characterization, and exploration of their biological potential. *International Journal of Chemical Studies*, *12*, 131–134.

Raina, S., & Klein, G. (2025). Lipopolysaccharide: recent advances in its biosynthesis and controlling cell envelope homeostasis. *International Journal of Molecular Sciences*, *26*(16), 7705.

Sarwade, K. N., Thakur, S. V., Sakhare, K. B., Sakhare, M. A., & Bharate, Y. N. (2025). Anti-alzheimer's, anticancer, and antimicrobial activities of transition metal complexes of 4-[(E)-(5-chloro-2-hydroxy-3-{(E)-(3-nitrophenyl) diazenyl} benzylidene) amino]-1, 5-dimethyl-2-phenyl-1H-pyrazol-3 (2H)-one. *Current Bioactive Compounds*, 21(8), E15734072349875.

Schatz, A., Martin, J. J., Fosdick, L. S., & Leicester, H. M. (1962). The proteolysis-chelation theory of dental caries. *The Journal of the American Dental Association*, *65*(3), 368–375.

Shu, S., & Mi, W. (2022). Regulatory mechanisms of lipopolysaccharide synthesis in Escherichia coli. *Nature Communications*, *13*(1), 1–11.

Singha, U. K., Pradhan, S., Mishra, D. K., Gurung, P., Chettri, A., & Sinha, B. (2023). Synthesis, physicochemical characterisation and DNA binding study of a novel azo Schiff base Ni(II) complex. *European Journal of Chemistry*, *14*(2), 280–286.

Siotey, A., Jain, P., Singhania, U., Pathan, E. K., & Sonawane, S. L. (2025). Tailor-made chitosan-azovanillin photochromic Schiff bases for antimicrobial applications. *ACS Applied Bio Materials*, *8*(7), 6368–6378

Subha, L., Balakrishnan, C., Natarajan, S., Theetharappan, M., Subramanian, B., & Neelakantan, M. A. (2016). Water soluble and efficient amino acid Schiff base receptor for reversible fluorescence turn-on detection of Zn^{2+} ions: Quantum chemical calculations and detection of bacteria. *Spectrochimica Acta Part A: Molecular and Biomolecular Spectroscopy*, *153*, 249–256.

Waszkowska, K., Busch, M., Slassi, S., Amine, A., El-Ghayoury, A., Strzelecki, J., Zawadzka, A., Kityk, A. V, Huber, P., & Sahraoui, B. (2025). Transition-metal azo Schiff base complexes: Nonlinear optics across solutions, thin films and nanocomposites. *Advanced Optical Materials*, *13*(30), e00975.